Applied Catalysis B: Environmental 123–124 (2012) 117–126

Contents lists available at SciVerse ScienceDirect

Applied Catalysis B: Environmental

journal homepage: www.elsevier.com/locate/apcatb

Fenton-like degradation of 2,4-dichlorophenol using Fe_3O_4 magnetic nanoparticles

Lejin Xu[a], Jianlong Wang[a,b,*]

[a] Laboratory of Environmental Technology, INET, Tsinghua University, Beijing 100084, PR China
[b] Beijing Key Laboratory of Fine Ceramics, Tsinghua University, Beijing 100084, PR China

ARTICLE INFO

Article history:
Received 21 January 2012
Received in revised form 26 March 2012
Accepted 20 April 2012
Available online 27 April 2012

Keywords:
Fe_3O_4 magnetic nanoparticles
Hydrogen peroxide
Fenton-like
2,4-Dichlorophenol
Hydroxyl radicals

ABSTRACT

Fenton-like degradation of 2,4-dichlorophenol (2,4-DCP) in aqueous solution was investigated over Fe_3O_4 magnetic nanoparticles (MNPs) as catalyst. The obtained samples were characterized by X-ray diffraction (XRD), high-resolution transmission electron microscopy (HRTEM), X-ray photoelectron spectroscopy (XPS), nitrogen adsorption–desorption isotherms, and physical property measurement system (PPMS). The catalytic results showed that Fe_3O_4 MNPs presented good properties for the degradation and mineralization of 2,4-DCP, achieving complete decomposition of 2,4-DCP and 51% of TOC removal after 180 min at reaction conditions of H_2O_2 12 mM, Fe_3O_4 MNPs 1.0 g/L, 2,4-DCP 100 mg/L, pH 3.0 and T 30 °C. The effect of different reaction parameters such as initial pH, H_2O_2 dosage, Fe_3O_4 MNPs addition, initial concentration of 2,4-DCP and temperature on two-stage first-order kinetics of 2,4-DCP degradation was studied. A high utilization efficiency of H_2O_2 calculated as 73% was observed. According to the analyses of iron leaching, reactive oxidizing species and degradation intermediates, a possible mechanistic steps of 2,4-DCP degradation dominated by $^{\bullet}OH$ reactions (especially by free $^{\bullet}OH$ in the bulk solution) were proposed. Besides, stability and reusability of Fe_3O_4 MNPs were tested.

1. Introduction

Fenton-like process using solid catalysts, which can generate strong oxidants capable of decomposing recalcitrant organic contaminants, provides a promising alternative for the oxidative treatment of polluted soil and water. In recent years, zero-valent iron [1,2], iron-based clays, silicas and zeolites [3,4], iron containing materials [5,6], and iron oxide minerals [7–10] as heterogeneous Fenton-like catalysts have been studied. Among these catalysts, iron oxide minerals, such as magnetite (Fe_3O_4), hematite (α-Fe_2O_3) and goethite (α-FeOOH), are of great fundamental and technological importance because of their relative wide availability and specific structural, magnetic and catalytic properties [7,8,11].

The mechanism through the decomposition of hydrogen peroxide (H_2O_2) by pure iron oxides has been proposed in the literature [3,12–14]. Under acidic conditions, the process involves the redox recycling of Fe(II)/Fe(III) both at the surface of catalysts and in the bulk solution. A complex on the oxide surface, assigned as $\equiv Fe^{II}{\cdot}H_2O_2$, is initially formed by ligand displacement between the hydrous surface of $\equiv Fe^{II}{\cdot}H_2O$ and H_2O_2, producing hydroxyl radicals ($^{\bullet}OH$) by intramolecularly electron transfer, as seen in Eq. (1).

The surface Fe^{III} is reduced to Fe^{II} via reactions (2) and (3). The dissolved iron resulted from dissolution of iron oxides also initiates H_2O_2 decomposition in the bulk solution, which proceeds through a chain reaction (4)–(6), analogous to the Haber–Weiss mechanism [15]. These hydroxyl radicals produced both on the oxide surface and in the bulk solution are the main oxidants for the degradation of contaminants. At circumneutral pH values, the contribution of dissolved iron to H_2O_2 activation is minimal, and a different oxidative species such as high-valent iron (i.e., $\equiv Fe^{IV}$) may be formed as shown in Eqs. (7)–(9) [14].

$$\equiv Fe^{II}{\cdot}H_2O + H_2O_2 \rightarrow \equiv Fe^{II}{\cdot}H_2O_2 \rightarrow \equiv Fe^{III} + {}^{\bullet}OH + OH^- \quad (1)$$

$$\equiv Fe^{III} + H_2O_2 \rightarrow \equiv Fe^{III}{\cdot}H_2O_2 \rightarrow \equiv Fe^{II} + HOO^{\bullet} + H^+ \quad (2)$$

$$\equiv Fe^{III} + HOO^{\bullet} \rightarrow \equiv Fe^{II} + O_2 + H^+ \quad (3)$$

$$Fe^{II} + H_2O_2 \rightarrow Fe^{III} + {}^{\bullet}OH + OH^- \quad (4)$$

$$Fe^{III} + H_2O_2 \rightarrow Fe^{II} + HOO^{\bullet} + H^+ \quad (5)$$

$$Fe^{III} + HOO^{\bullet} \rightarrow Fe^{II} + O_2 + H^+ \quad (6)$$

$$\equiv Fe^{II} + H_2O_2 \rightarrow \equiv Fe^{IV} + 2OH^- \quad (7)$$

$$\equiv Fe^{IV} + H_2O_2 \rightarrow \equiv Fe^{II} + O_2 + 2H^+ \quad (8)$$

$$\equiv Fe^{IV} + \equiv Fe^{II} \rightarrow 2\equiv Fe^{III} \quad (9)$$

Magnetite (Fe_3O_4) has been observed to have especially efficient catalysis in Fenton-like system which is assigned to the presence

* Corresponding author at: Neng Ke Lou, Tsinghua University, Beijing 100084, PR China. Tel.: +86 10 62784843; fax: +86 10 62771150.
E-mail address: wangjl@tsinghua.edu.cn (J. Wang).

0926-3373/$ – see front matter © 2012 Elsevier B.V. All rights reserved.
http://dx.doi.org/10.1016/j.apcatb.2012.04.028

of Fe^{II} species in magnetite structure initiating the Fenton reaction [13]. With an inverse spinel crystal structure, it exhibits unique electric and magnetic properties based on the transfer of electrons between ferrous ions and ferric ions in the octahedral sites [16]. What is more, the high catalytic activity of nanoparticles has attracted more attention due to their high surface area and uniform pore size distribution [11]. Researchers have shown that Fe_3O_4 nanoparticles can be implicated as a heterogeneous Fenton-like catalyst for removal of environmental contaminants, including phenol [7,17], aniline [17], p-nitrophenol [11], pentachlorophenol [18], and 17α-methyltestosterone [13]. However, no study has been reported on Fe_3O_4 magnetic nanoparticles (MNPs) for Fenton-like degradation of 2,4-dichlorophenol (2,4-DCP). Much work is still needed to explore the reaction kinetics and degradation mechanism so that the heterogeneous Fenton operation can be transformed into an efficient process suitable for practical applications.

The compound under study (2,4-DCP) is used in large amounts in the production of some herbicides and preservatives, such as 2,4-dichlorophenoxyacetic acid and pentachlorophenol. The aim of this paper is to assess the catalytic performances of Fe_3O_4 MNPs for 2,4-DCP degradation, and to study the effect of initial conditions, such as pH, H_2O_2 and Fe_3O_4 MNPs dosage, 2,4-DCP concentration as well as reaction temperature. The kinetics of the catalytic reaction, degradation mechanism and the reusability of Fe_3O_4 MNPs were also evaluated.

2. Materials and methods

2.1. Reagents

Ferrous sulfate ($FeSO_4{\cdot}7H_2O$, Shenyang Reagent Factory), ferric sulfate ($Fe_2(SO_4)_3$, Tianjin Yongda Chemical Reagent Co., Ltd.), and NaOH (Beijing Chemical Factory) for preparation of Fe_3O_4 MNPs were of analytical grade and used without further purification. 2,4-Dichlorophenol was obtained from Beijing Jinlong Chemical Reagent Co. Ltd., and its degradation intermediates (2-chlorohydroquinone and 4,6-dichlororesorcinol) were purchased from J&K Scientific Ltd. Carboxylic acids, H_2O_2 (30%, v/v), H_2SO_4, *n*-butanol, KI, methanol and ethanol were supplied by Beijing Chemical Factory. Argon (Ar) gas (Beijing Aolin Gas Company) was supplied, and double distilled water was employed.

2.2. Preparation and characterization of MNPs

Fe_3O_4 MNPs used in this study were synthesized by coprecipitation of Fe(II) and Fe(III) in basic solutions in argon based on Massart's method [19–21]. A mixture solution of 100 mL 0.01 M $FeSO_4{\cdot}7H_2O$ and 0.02 M $Fe_2(SO_4)_3$ with 0.2 mL H_2SO_4 was added dropwise to 100 mL 0.2 M NaOH solution. After 1.5 h of vigorous stirring under an Ar stream at 80 °C, the precipitate was deposited and then washed with deionized water and ethanol for two times. Finally, MNPs were dried at room temperature under vacuum and then stored in desiccator for further experiments.

X-ray powder diffraction (XRD) measurement was carried out at room temperature on an XRD diffractometer (D8-Advance, Bruker) with Cu-Kα radiation at 40 kV and 40 mA. The morphology of the catalyst was determined by high-resolution transmission electron microscopy (HRTEM, Tecnai G2 F20 S-Twin). X-ray photoelectron spectroscopy (XPS) measurement was performed using a PHI-5300 system with Al Kα radiation (1486.6 eV), and the XPSPEAK4.1 software was used for data analysis. Before each measurement, the sample was out-gassed in a vacuum oven at 80 °C for 5 h, and the Brunauer–Emmett–Teller (BET) surface area was examined by nitrogen adsorption–desorption isotherm measurements at 77 K on a NOVA 3200e surface area and porosity analyzer. Magnetic measurement was performed at room temperature with a physical property measurement system (PPMS, 730T, LAKESHORE, USA).

2.3. Experimental procedure

All experiments were conducted in the dark in a conical flask (25 mL) placed in a thermostated water bath (TZ-2EH, Beijing Wode Company) with an agitation of 150 rpm. The reactions were initiated by adding a desired dosage of H_2O_2 to a pH-adjusted solution by H_2SO_4 containing Fe_3O_4 MNPs and the probe compound 2,4-DCP. Samples were withdrawn at predetermined time intervals, and filtered immediately through a 0.22 μm filter film. Meanwhile, 10 μL 1 M *n*-butanol was added into 1 mL sample to quench the reaction. The reusability of the catalyst was evaluated by collecting with a magnet, washing with deionized water, drying the used catalyst under vacuum, and using it for the next reaction under similar experimental conditions. Experiments were carried out at least in duplicate, and all results were expressed as a mean value.

2.4. Sample analysis

The concentration of 2,4-DCP and its intermediates was measured by means of an Agilent 1200 high performance liquid chromatography (HPLC) with a C18 reversed-phase column (5 μm, 4.6 mm × 150 mm) and a diode array detector (DAD). The mobile phase was methanol/water (60:40, v/v) with a flow rate of 1.0 mL/min. The UV detector was set at 284 nm for 2,4-DCP and 4,6-dichlororesorcinol, and 254 nm for 2-chlorohydroquinone.

Total organic carbon (TOC) was analyzed using a Multi TOC/TN Analyzer (2100, Analytik Jena AG Corporation). The solution pH was measured by a Thermo Orion model 8103BN pH-meter. To determine the concentration of chloride ions (Cl^-) and carboxylic acids, an ion chromatography (DX-100, Dionex, Germany) equipped with a Dionex RFIC™ IonPac® AS 14 analytical column (4 mm × 250 mm) and a Dionex RFIC™ IonPac® AG 14 guard column (4 mm × 50 mm) was used throughout the experiment. The eluent was 3.5 mM Na_2CO_3 and 1.0 mM $NaHCO_3$ with a flow rate of 1.0 mL/min.

Ferrous ion and total dissolved iron concentrations were measured according to the 1,10-phenanthroline method [14,22,23], using a Lambda 25 UV/vis spectrophotometer (PerkinElmer) at 510 nm. Hydrogen peroxide concentration in the solution was determined by iodometric titration method [24].

3. Results and discussion

3.1. Characterization of Fe_3O_4 MNPs

XRD patterns of the synthesized magnetite and commercial Fe_3O_4 powders are shown in Fig. 1a and b. The characteristic reflections of two materials were assigned to the (2 2 0), (3 1 1), (4 0 0), (5 1 1) and (4 4 0) planes of the cubic spinel structure with space group *Fd*-3*m* (2 2 7) corresponding to the standard card of magnetite (JCPDS No. 19-0629). From XRD reflections of Fe_3O_4 MNPs, a considerable degree of crystallization was observed. The broad XRD peaks indicated the small crystallite dimension of Fe_3O_4 MNPs. The average particle size of samples was calculated from the most intense (3 1 1) peak according to the Scherrer's equation, which was 5.7 and 28.5 nm for synthesized Fe_3O_4 MNPs and commercial Fe_3O_4 powders, respectively. As seen in the XRD patterns of reused Fe_3O_4 MNPs (Fig. 1c), there was no obvious change of characteristic peaks before and after oxidation reactions, and the (3 1 1) peak was slightly broader after five runs, which may result from the dissolution of solid.

Fig. 2a and b represents HRTEM images illustrating the particle size and morphology of the synthesized Fe_3O_4 MNPs and

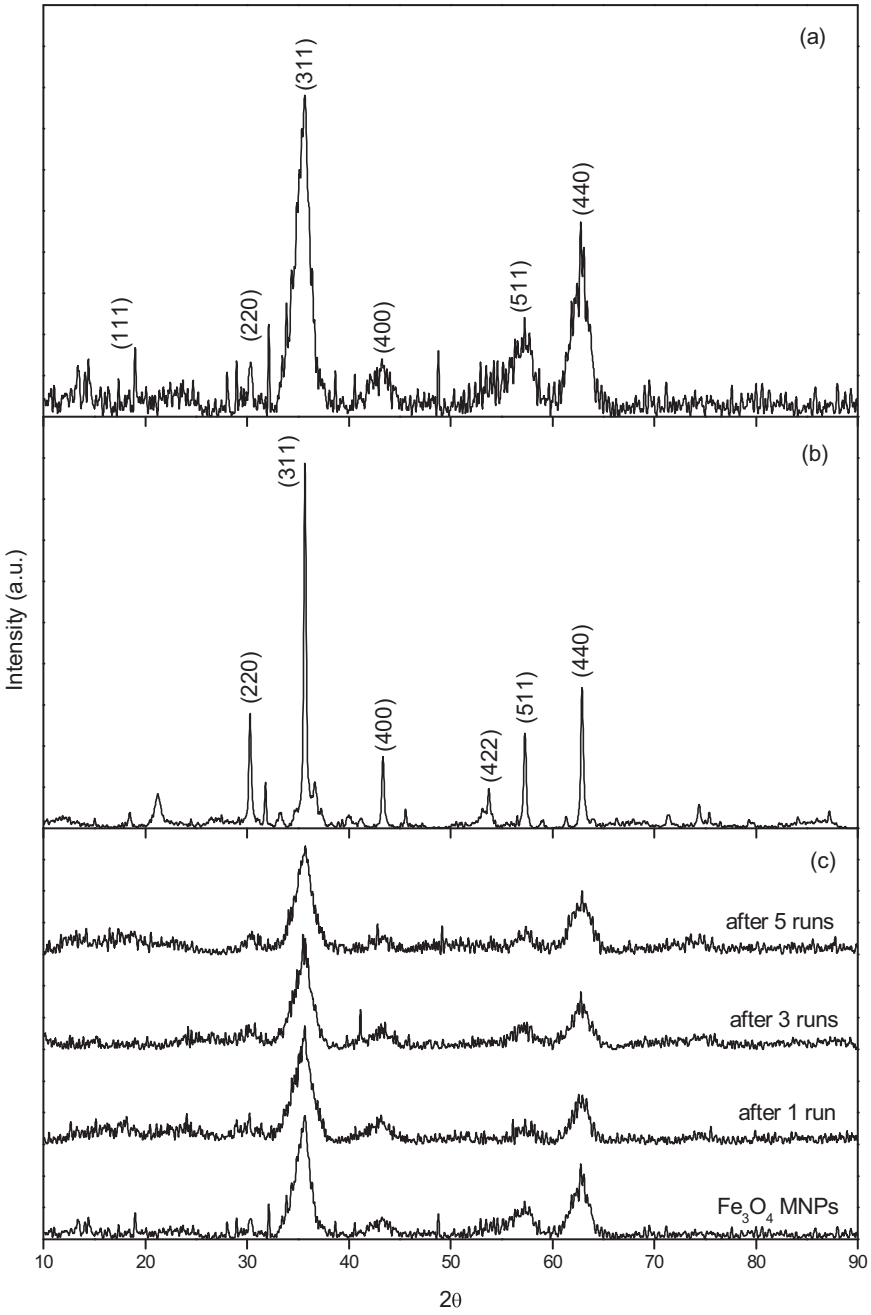

Fig. 1. XRD patterns of (a) synthesized Fe_3O_4 MNPs, (b) commercial Fe_3O_4 powders and (c) reused Fe_3O_4 MNPs.

commercial Fe_3O_4 powders, which are consistent with the results of XRD analysis. It can be seen that these synthesized Fe_3O_4 MNPs were very uniform with 10 nm in diameter, and commercial Fe_3O_4 powders were irregular and had much lager diameter. The image of Fe_3O_4 MNPs reused for five times in Fig. 2c showed the corrosion phenomenon of the catalyst after oxidation reaction, in accord with the observation results from XRD, which might cause the decrease of particle surface area and catalytic activity.

As-synthesized Fe_3O_4 MNPs were also characterized by XPS to confirm the metallic state of Fe as seen in Fig. 3. The binding energies of about 280, 530 and 711 eV indexed to C 1s, O 1s and Fe 2p, respectively, the corresponding atomic concentrations of which were 37.3%, 52.8% and 9.9%. The peaks located at about 711 and 725 eV represented the binding energies of Fe $2p_{3/2}$ and Fe $2p_{1/2}$, respectively, and the binding energies of 711.1 and 713.3 eV indicated the presence of Fe(II) and Fe(III), consistent with the literature data for magnetite [13,25].

The specific surface area of Fe_3O_4 MNPs calculated based on BET method was 67.8 m^2/g. The average pore diameter was found to be 3.8 nm, which indicated that the Fe_3O_4 MNPs was mesoporous according to the definition of pore size by International Union of Pure and Applied Chemistry (IUPAC). As illustrated in Fig. 4, the N_2 adsorption/desorption isotherms for the Fe_3O_4 MNPs were classified as IUPAC type IV, which further confirmed the mesoporous structure.

Fig. 5 shows the magnetization curves measured at room temperature for the synthesized Fe_3O_4 MNPs before and after Fenton-like reactions. No magnetic hysteresis loop appeared, exhibiting superparamagnetic property with a saturation magnetization (M_s) of 19.6 emu/g for Fe_3O_4 MNPs. This specific M_s value

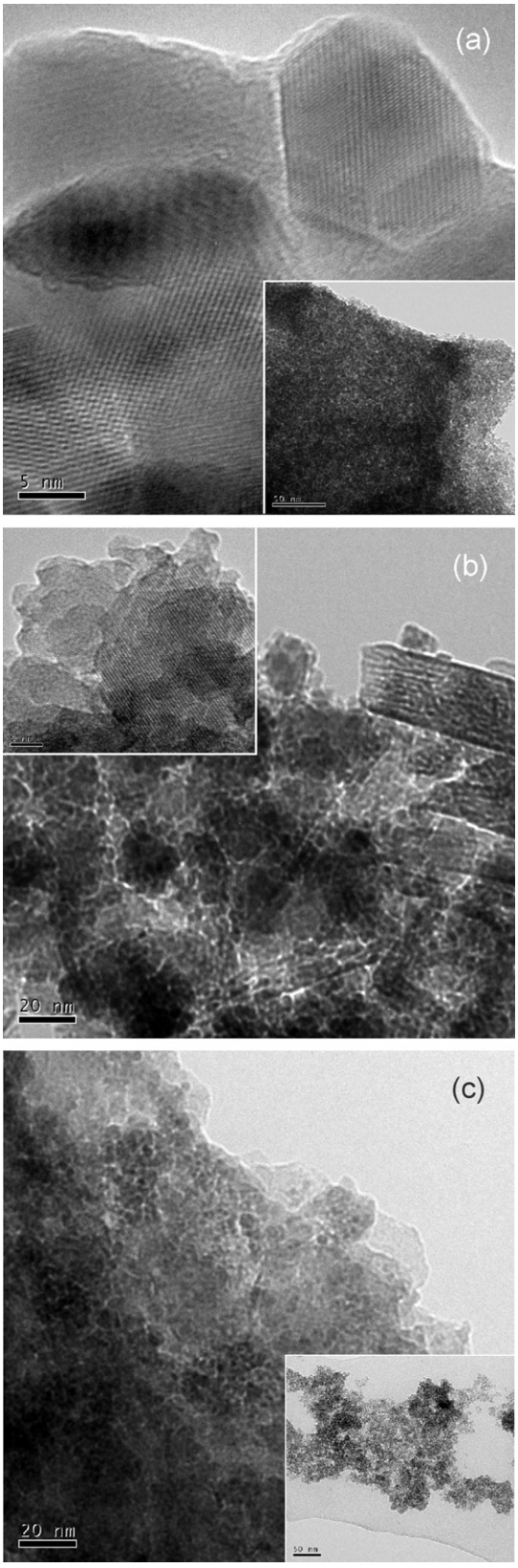

Fig. 2. HRTEM micrographs of (a) synthesized Fe_3O_4 MNPs, (b) commercial Fe_3O_4 powders and (c) reused Fe_3O_4 MNPs for five times.

is lower than those reported for bulk magnetite (92 emu/g) due to the smaller particle size and the surface-related effects such as surface disorder [26–28]. After 5 reactions for 2,4-DCP removal, the saturation magnetization became higher with M_s of 23.1 emu/g, indicating that the Fe_3O_4 MNPs can be easily separated and recovered from solution by an external magnetic field such as a magnet (Fig. 5, inset) after their uses.

3.2. Catalytic property of Fe_3O_4 MNPs

The degradation of 2,4-DCP along time under different experimental conditions was evaluated as shown in Fig. 6. It was observed that within 180 min reaction the concentration of 2,4-DCP diminished very slowly with only 30 mM H_2O_2, and even throughout 24 h only 13% removal was obtained (the inset of Fig. 6), which is ascribed to the weak oxidation potential of H_2O_2 compared with hydroxyl and perhydroxyl radicals [13]. Less than 15% degradation of 2,4-DCP was observed in control reactions with 1.5 g/L Fe_3O_4 MNPs, and about 0.027 mM free chloride was detected in the solution after 24 h reaction, which was mainly expected to surface adsorption as well as reductive dechlorination [11]. However, rapid degradation of 2,4-DCP was achieved in the Fenton-like system catalyzed by Fe_3O_4 MNPs with initial parameters of pH 3.0, 1.0 g/L catalyst and 12 mM H_2O_2, indicating the high catalytic ability of Fe_3O_4 MNPs to the H_2O_2 activation. The comparison of Fe_3O_4 MNPs with commercial Fe_3O_4 powders was investigated under similar reaction conditions, the result of which showed that synthesized Fe_3O_4 MNPs were much more efficient. The performance of the commercial Fe_3O_4 powders could be ascribed to the larger particle diameter and irregular size as characterized by XRD and HRTEM which offered less active sites for H_2O_2 decomposition.

3.3. Investigation into two-stage first-order kinetics of 2,4-DCP degradation

As the 2,4-DCP degradation kinetics was significantly influenced by different initial parameters, i.e., pH, H_2O_2 dosage, Fe_3O_4 MNPs addition, initial 2,4-DCP concentration and temperature, a series of comparative experiments were conducted as shown in Figs. 7 and 8. It should be noticed that an induction period (first-stage) and a followed rapid degradation stage (second-stage) exhibited apparent first-order kinetics were observed in the degradation of 2,4-DCP in pH 2.0 and 3.0 experiments, which was also investigated by many other researchers [29–31]. Gordon and Marsh [30] found that degradation kinetics of 2-chlorophenol was modeled as a pseudo-first-order reaction with two stages at pH 3.0.

3.3.1. Effect of pH

It can be seen from Fig. 7a that pH has a decisive influence on the removal of 2,4-DCP by Fenton-like reaction. The experiments were carried out at five different pH values of 2.0, 3.0, 3.9, 4.6 and 5.0, and the results showed that slow degradation of 2,4-DCP was observed at pH values of 3.9, 4.6 and 5.0, while a lower pH caused a shorter induction time and a higher kinetic rate (k) of second-stage. The kinetic constants of second-stage at pH 2.0 and 3.0 were 0.175 and 0.064 min^{-1}, respectively, which had the similar magnitude with the k of the homogeneous Fenton system reported by Oliveira et al. [32]. The increased oxidation efficiency at lower pH values can be attributed to the higher oxidation potential of hydroxyl radicals, the more dissolved fraction of iron species, the stability of H_2O_2 in acidic solution that can not be decomposed immediately to H_2O and O_2, and the formation of metal oxide–pollutant inner-sphere complexes that will promote reaction [17,33,34].

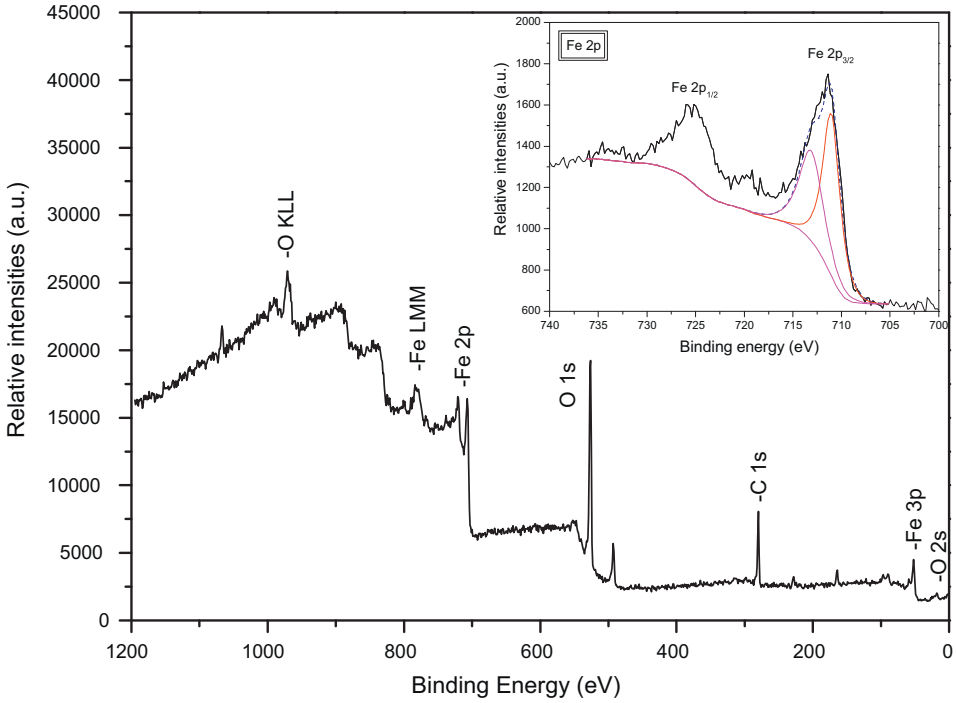

Fig. 3. XPS spectra of the Fe_3O_4 MNPs and the high-resolution scan of Fe 2p region (inset).

3.3.2. *Effect of H_2O_2 dosage*

The oxidation of 2,4-DCP over 1.0 g/L Fe_3O_4 MNPs at pH 3.0 with different H_2O_2 concentrations were investigated as shown in Fig. 7b. The marked effect of H_2O_2 concentration on 2,4-DCP degradation was not obtained, and even with 0.6 mM H_2O_2, the kinetic rate of second-stage was still high. When H_2O_2 concentration increased from 0.6 to 12 mM, the induction period was shortened from about 94 to 64 min, and further increase of H_2O_2 concentration (30 mM) inhibited the degradation with k (second-stage) decreasing from 0.064 (12 mM) to 0.046 min^{-1} (30 mM). The occurrence of the maximum H_2O_2 concentration of 12 mM can be explained by the scavenging effect of $^{\bullet}OH$ by H_2O_2 as expressed by reaction (10) [2,13]. Although other oxidants like $HOO^{\bullet}$ and $O_2^{\bullet-}$ are generated, they have much lower oxidation potentials than $^{\bullet}OH$ and do much less contribution to 2,4-DCP degradation [35].

$$^{\bullet}OH + H_2O_2 \rightarrow H_2O + HOO^{\bullet} \quad (10)$$

$$HOO^{\bullet} \leftrightarrow O_2^{\bullet-} + H^{+} \ (pK_a 4.8) \quad (11)$$

3.3.3. *Effect of Fe_3O_4 MNPs addition*

Fig. 7c illustrates the effect of Fe_3O_4 MNPs dose on the two-stage degradation kinetics with initial 2,4-DCP concentration 100 mg/L and H_2O_2 dosage 12 mM at pH 3.0 and temperature 30 °C. The increase of Fe_3O_4 MNPs addition from 0.2 to 1.5 g/L obviously shortened the induction time and increased the kinetic rate of second-stage, which indicated that increasing amount of

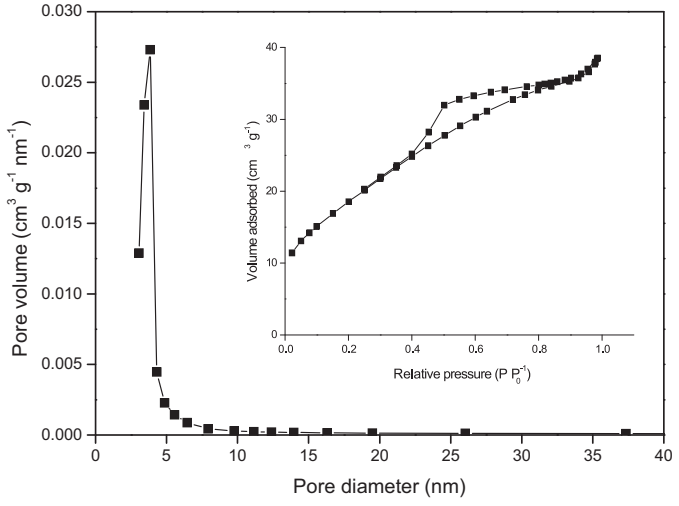

Fig. 4. Nitrogen adsorption/desorption isotherms (inset) and pore size distribution of Fe_3O_4 MNPs.

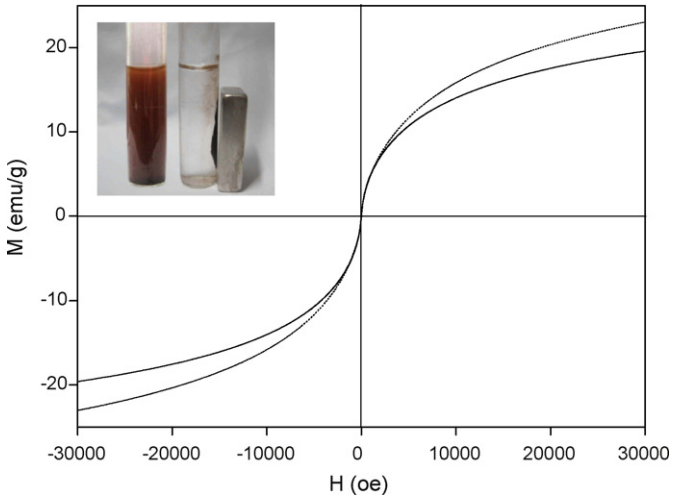

Fig. 5. Magnetization curves measured at room temperature for the synthesized Fe_3O_4 MNPs before (solid line) and after 5 reactions (dashed line), and the photograph of the sample attracted by a magnet (inset).

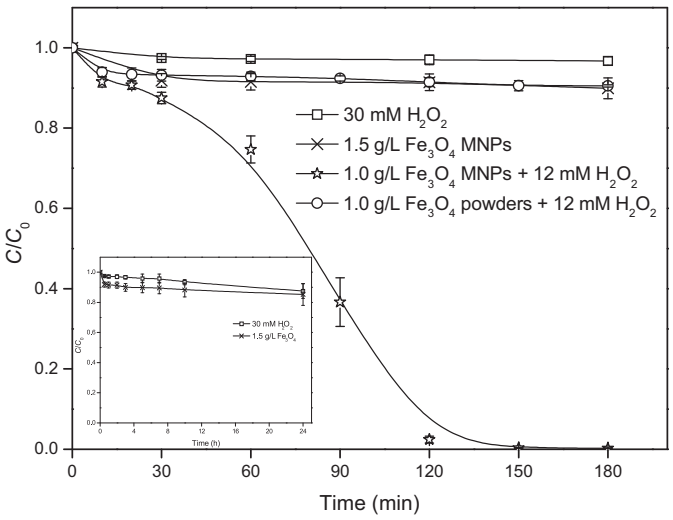

Fig. 6. The degradation of 100 mg/L 2,4-DCP at the initial pH 3.0 and 30 °C under different conditions. Inset graph is the result of 2,4-DCP degradation conducted in Fe_3O_4 MNPs (1.5 g/L) alone and H_2O_2 (30 mM) alone throughout 24 h reaction time.

active sites on oxide surface accelerated the reactions of H_2O_2 decomposition and iron dissolution producing more •OH [13,36]. Nevertheless, when Fe_3O_4 MNPs addition was further increased to 2.0 g/L, the degradation of 2,4-DCP was not enhanced but slightly decreased with k (second-stage) decreasing from 0.066 (1.5 g/L) to 0.065 min^{-1} (2.0 g/L), because of the agglomeration of nanoparticles and the scavenging of hydroxyl radicals or other radicals by present iron species through undesirable reactions (12)–(14) [35,37].

$$^{\bullet}OH + Fe^{II} \rightarrow OH^{-} + Fe^{III} \quad (12)$$

$$HOO^{\bullet} + Fe^{II} \rightarrow OOH^{-} + Fe^{III} \quad (13)$$

$$HOO^{\bullet} + Fe^{III} \rightarrow Fe^{II} + O_2 + H^{+} \quad (14)$$

3.3.4. *Effect of initial concentration of 2,4-DCP*

The results for reaction kinetics as a function of 2,4-DCP initial concentration ranging from 20 to 100 mg/L at various reaction times with H_2O_2 dosage 12 mM and Fe_3O_4 MNPs 1.0 g/L at pH 3.0 and temperature 30 °C are displayed in Fig. 7d. The induction time was slightly shortened, and the kinetic rate of second-stage was increased from 0.033 to 0.064 min^{-1} with the increase of its initial concentration from 20 to 100 mg/L. This phenomenon may be ascribed to the excessive dosage of H_2O_2 and Fe_3O_4 MNPs for

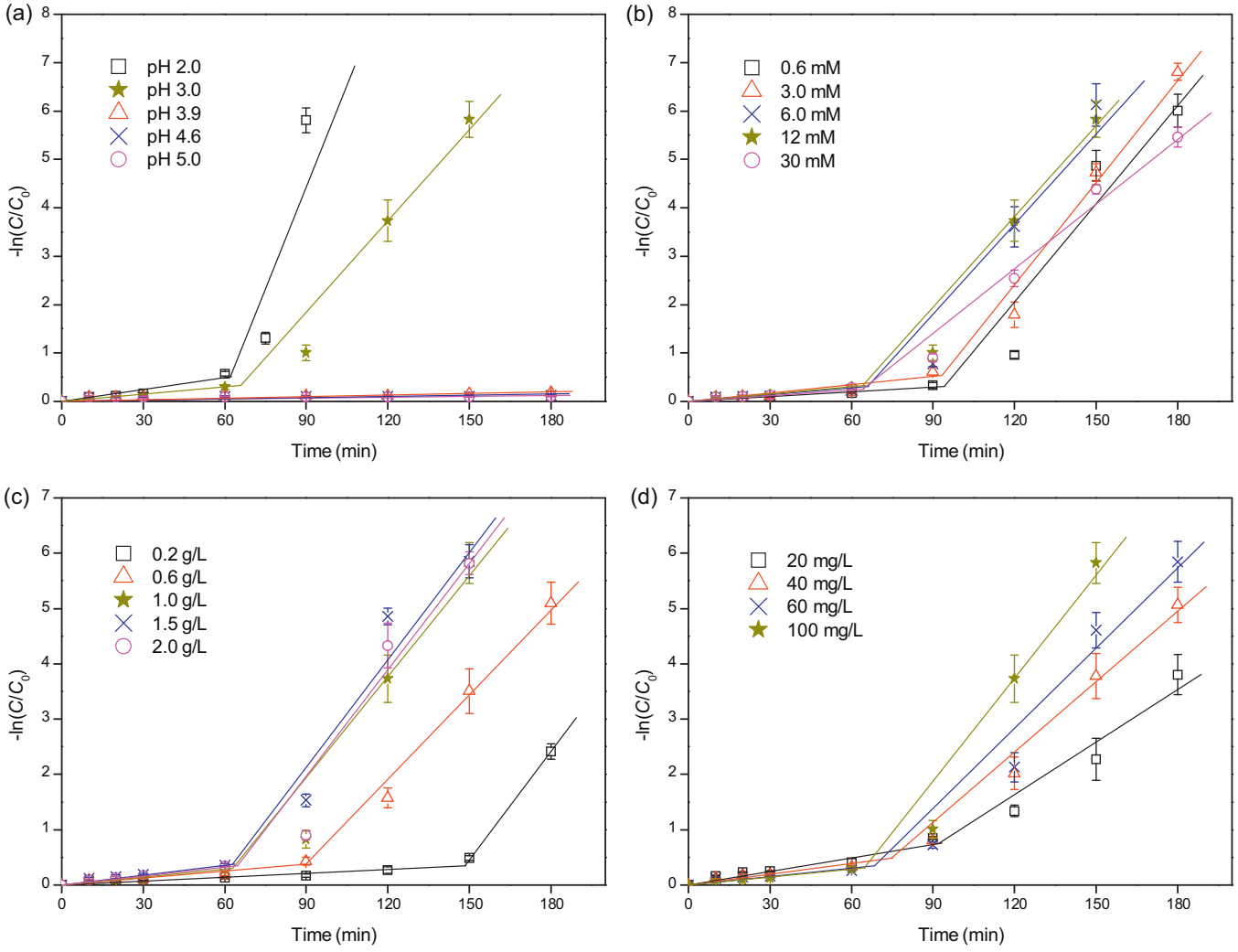

Fig. 7. Influence of different initial parameters on 2,4-DCP degradation in the Fenton-like process catalyzed by Fe_3O_4 MNPs: (a) pH; (b) H_2O_2 dosage; (c) Fe_3O_4 MNPs addition; (d) initial 2,4-DCP concentration. Except for the investigated parameter, other parameters fixed on pH 3.0, H_2O_2 12 mM, Fe_3O_4 MNPs 1.0 g/L, 2,4-DCP 100 mg/L and temperature 30 °C.

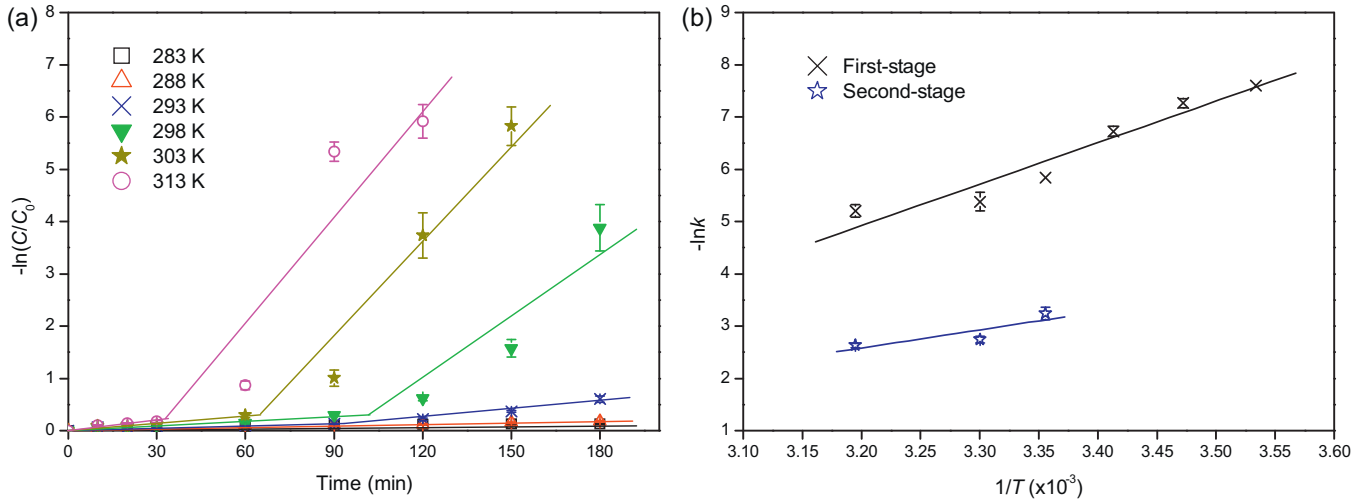

Fig. 8. Effect of temperature on 2,4-DCP degradation (a) and Arrhenius plots for Fe_3O_4 MNPs catalyzed reaction (b) carried out at pH 3.0 with H_2O_2 12 mM, Fe_3O_4 MNPs 1.0 g/L and 2,4-DCP 100 mg/L.

lower initial concentration of 2,4-DCP resulting in the scavenging of oxidative radicals as described in former sections.

3.3.5. *Effect of temperature*

The apparent rate constants of 2,4-DCP degradation were also determined at selected reaction temperatures to investigate the activation energy of the reaction on the Fe_3O_4 surface. As shown in Fig. 8a, the time of induction period is greatly decreased with the increase of temperature from 283 to 313 K, possibly signifying that the dissolution of Fe_3O_4 MNPs in the first-stage is an endothermic process [30]. The increase in rate constant of second-stage with temperature could be attributed to the exponentially increasing kinetic constants for both Fe^{II}/Fe^{III} regeneration and radical production [38,39]. The apparent activation energies were calculated from these rate constants of two stages identified at the selected reaction temperatures, and Arrhenius plots for Fe_3O_4 MNPs catalyzed reactions are shown in Fig. 8b. It should be noted that the reactions at temperatures of 283, 288 and 293 K are very slow, which are excluded from the calculation of the apparent activation energy in second-stage. According to Arrhenius equation $k = A \times \exp(-E_a/RT)$, the activation energy (E_a) of first-stage was calculated as 66.0 kJ/mol, while for the second region of reaction, E_a was 28.8 kJ/mol. The E_a values are higher than that of the diffusion-controlled reactions (ranged within 10–13 kJ/mol), which indicates that the apparent reaction rate is dominated by the rate of intrinsic chemical reactions on the oxide surface rather than the rate of mass transfer [12]. The apparent activation energy determined for the second-stage is closer to E_a reported for the homogeneous Fenton reaction that is 34.8 kJ/mol for acidic oxidation of Orange G [40], suggesting that hydroxyl radicals produced through a Fenton reaction in the bulk solution (Eqs. (4)–(6)) play a significant role in the second stage of 2,4-DCP degradation.

As suggested by previous studies, the reaction involving the dissolution of Fe_3O_4 MNPs is the rate-determining step of this reaction

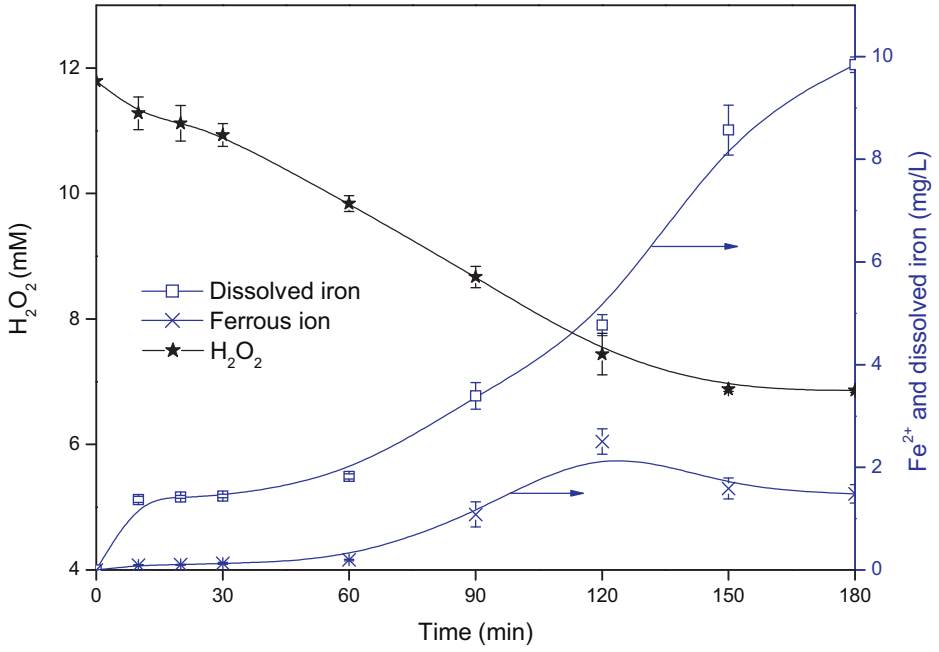

Fig. 9. Investigation of H_2O_2 decomposition and iron dissolution during 2,4-DCP degradation with H_2O_2 12 mM, Fe_3O_4 MNPs 1.0 g/L and 2,4-DCP 100 mg/L at pH 3.0 and T 30 °C.

[30]. It can be concluded that an slow transfer of iron from the surface of Fe_3O_4 MNPs into the solution exists in the first-stage, and the induction period may be due to the fact that the activation of H_2O_2 by Fe_3O_4 MNPs does not seem to produce an appreciable amount of efficacious •OH that is the main oxidant for 2,4-DCP degradation [9]. The •OH formed on the catalyst surface may be at an important rate, but they are recombined (Eq. (15)) or scavenged quickly by high concentration of H_2O_2 (Eq. (10)) and large activated area of Fe_3O_4 MNPs (Eq. (12)) before becoming available to oxidize 2,4-DCP [2,41]. The second stage predominantly involves the reaction of 2,4-DCP with hydroxyl radicals produced by reaction with dissolved iron species (Eq. (4)). These results can be further supported by the variation of dissolved iron, ferrous ion and H_2O_2 described in Section 3.4 and the effect of radical scavengers discussed in detail in Section 3.5.

$$^{\bullet}OH + {}^{\bullet}OH \rightarrow H_2O_2 \quad (15)$$

3.4. Iron leaching and H_2O_2 decomposition

The Fe ions concentration and the decomposition of H_2O_2 in the 2,4-DCP aqueous solution were investigated with H_2O_2 12 mM, Fe_3O_4 MNPs 1.0 g/L and 2,4-DCP 100 mg/L at pH 3.0 and T 30 °C as shown in Fig. 9. Slow linear dissolution of iron in the first 60 min reaction was found, in accordance with the first-stage of kinetic degradation of 2,4-DCP. Afterwards a high concentration of ferrous (0.2–2.5 mg/L from 60 to 120 min) was observed, indicating that homogeneous Fenton reaction in the bulk solution is expected predominantly in the second-stage of 2,4-DCP degradation. The ferrous concentration reached a peak value at 120 min when 2,4-DCP was almost completely removed (Fig. 6), and then the concentration decreased to 1.5 mg/L after 180 min of reaction. As reported previously [29,42], the descending of ferrous concentration may be caused by the oxidation of ferrous ions into ferric ions by remaining oxidants (such as •OH and H_2O_2) in the solution. However, the concentration of total dissolved iron increased as reaction time increased and the descending period did not occur, which could be attributed to the continuous leaching of iron from Fe_3O_4 MNPs. About 9.8 mg/L of the iron dissolved into solution after 180 min, equivalently 9.8% of total iron of 1.0 g/L catalyst used.

It can also be seen that the concentration of H_2O_2 decreased gradually during the degradation of 2,4-DCP. The mineralization of one mole 2,4-DCP consumes 12 moles of H_2O_2 in stoichiometry, as expressed in Eq. (16). Based on the study of Luo et al. [6], the utilization efficiency of H_2O_2 can be calculated by the ratio of H_2O_2 amount used for 2,4-DCP degradation against the total amount of the consumed H_2O_2 in the reaction. About 51% TOC removal was achieved as seen in Section 3.5, which could be used for calculation of the H_2O_2 amount for 2,4-DCP degradation. As shown in Fig. 9, about 4.9 mM H_2O_2 was consumed during 180 min reaction. Thus, the utilization efficiency of H_2O_2 was calculated as 73% in our system.

$$C_6H_4OCl_2 + 12H_2O_2 \rightarrow 6CO_2 + 13H_2O + 2HCl \quad (16)$$

3.5. Analyses of reactive oxidizing species, degradation intermediates and reaction mechanism

To discriminate the reactive oxidizing species for 2,4-DCP degradation, *n*-butanol and iodide ion were used to scavenge all the •OH produced in the process and surface-bounded •OH formed at the surface of Fe_3O_4 MNPs, respectively [2,43,44]. The degradation of 2,4-DCP was almost completely inhibited by excess *n*-butanol (300 mM) as shown in Fig. 10a, indicating that free radicals including surface-bounded •OH and free •OH in the bulk solution have a dominant role in the decomposition of 2,4-DCP. In the presence of 10 mM KI, the degradation of 2,4-DCP was slightly inhibited and about 88% of 2,4-DCP removal was obtained after 180 min reaction, which suggested that surface-bounded •OH are minor oxidants for rapid degradation of 2,4-DCP. Therefore, 2,4-DCP was predominately oxidized by the attack of hydroxyl radicals, particularly •OH in the bulk solution, further confirming the investigation of degradation kinetics in Section 3.3.

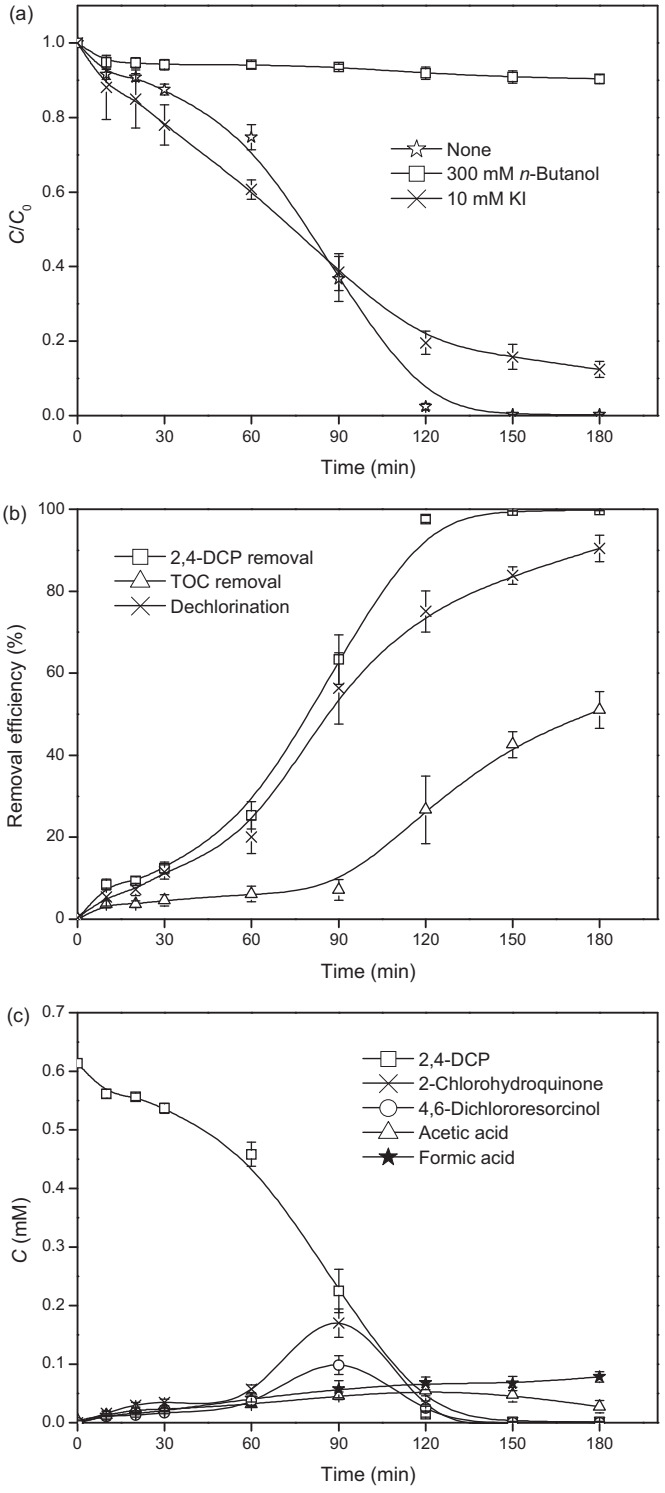

Fig. 10. (a) Effect of radical scavengers on the degradation of 2,4-DCP; (b) degradation efficiency, TOC removal and dechlorination of 2,4-DCP; (c) variation of the concentration of degradation intermediates detected by HPLC and IC. Reaction conditions: H_2O_2 12 mM, Fe_3O_4 MNPs 1.0 g/L, 2,4-DCP 100 mg/L, pH 3.0, T 30 °C.

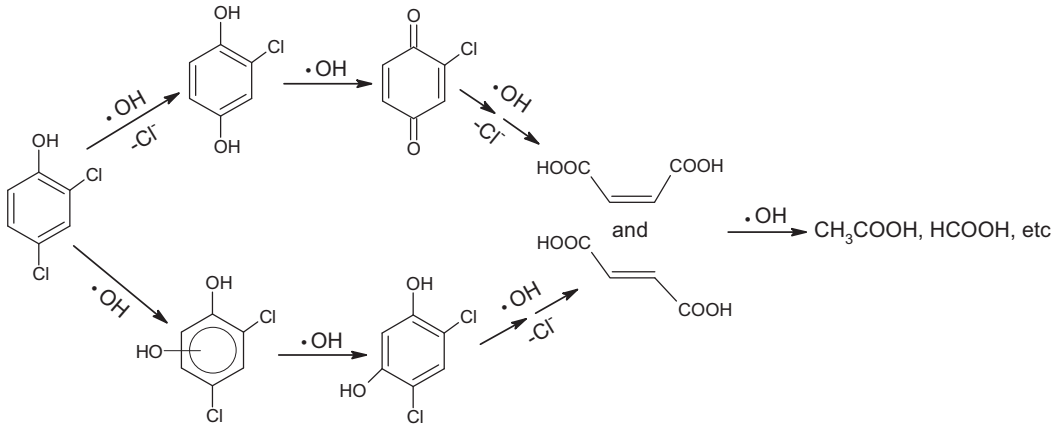

Fig. 11. Proposed reaction pathway for the mineralization of 2,4-DCP at pH 3.0 by Fenton-like process using Fe_3O_4 MNPs.

The decrease of TOC concentration was observed to evaluate the mineralization level of 2,4-DCP in our system as depicted in Fig. 10b. Firstly, TOC concentration decay was slow, and then 51% of TOC was removed at 180 min, indicating that some of the intermediates derived from 2,4-DCP decomposition such as carboxylic acids remained in solution. As chloride substituents are responsible to the toxicity of aromatic compounds, the dechlorination degree was also measured to estimate the detoxification degree. As seen in Fig. 10b, the dechlorination degree of 2,4-DCP reached 90%, showing that most of the chlorine on the aromatic ring was released and formed chloride ion. Through HPLC and IC analyses, the main intermediates were 2-chlorohydroquinone, 4,6-dichlororesorcinol, acetic acid and formic acid (see Fig. 10c). The concentration of aromatic intermediates increased slowly at first 60 min, reached a peak value at about 90 min, and then decreased till complete removal within 150 min. Acetic acid and formic acid were gradually formed and remained in solution after 180 min reaction. Although the dechlorination of 2,4-DCP to monochlorophenols and phenol has been reported by many researchers [45,46], 4-chlorophenol, phenol and hydroquinone were not detected in our system.

Considering the experimental results analyzed above and taking into account the information reported in the literature [47–50], a reaction pathway for the degradation of 2,4-DCP was proposed in Fig. 11. The chlorine atom located in the para-position on the aromatic ring was substituted by •OH to yield 2-chlorohydroquinone, which was apparently the preferred location for radical collisions on the 2,4-DCP because of the steric effect. This chlorinated hydroquinone may separate two hydrogen atoms with further attack of •OH to give 2-chloro-1,4-benzoquinone. Meanwhile, an electrophilic •OH group could be added onto the aromatic ring of the 2,4-DCP, resulting in the formation of hydroxylated products such as 4,6-dichlororesorcinol. Further oxidation with dechlorination of chlorobenzoquinone and 4,6-dichlororesorcinol yielded maleic and fumaric acids, which were degraded to smaller molecular organic acids such as acetic acid and formic acid remaining in solution eventually.

3.6. Catalytic stability of Fe_3O_4 MNPs

Successive experiments were performed in order to evaluate the possibility of catalyst reuse. From Fig. 12, it is obvious that the initial activity decreased gradually during five consecutive runs at similar reaction conditions of Fe_3O_4 MNPs 1.0 g/L, H_2O_2 12 mM, 2,4-DCP 100 mg/L, pH 3.0 and T 30 °C. This initial loss of activity can be ascribed to the decay of active catalytic sites caused by small amounts of leached iron from the catalyst surface as described in Section 3.4, which is further supported by the observation results

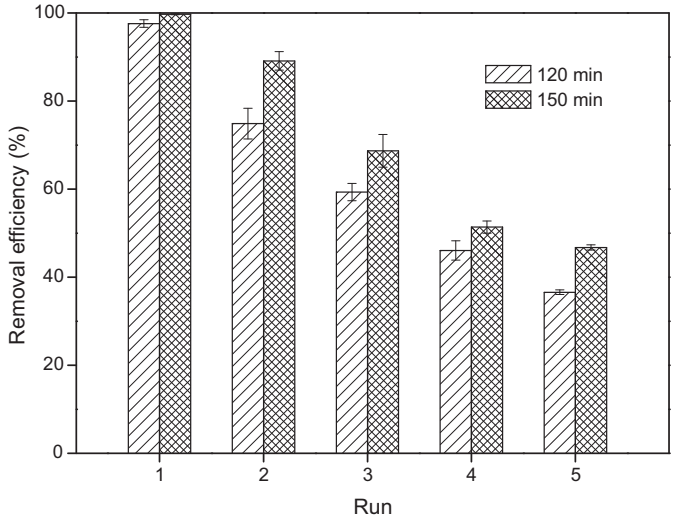

Fig. 12. Five consecutive experiments of the degradation of 2,4-DCP with 1.0 g/L reused Fe_3O_4 MNPs at reaction conditions of H_2O_2 12 mM, 2,4-DCP 100 mg/L, pH 3.0 and T 30 °C.

from XRD (Fig. 1c) and TEM (Fig. 2c) patterns of reused Fe_3O_4 MNPs. Similar results were observed by other authors who attributed the catalyst deactivation to a diversity of factors, including reduction of the catalyst specific area, poisoning of the active catalytic sites by adsorbed organic species, conglomeration of MNPs, and the discarding of supernatants during the rinsing of MNPs [17,51]. More work is needed to explore the causes of catalyst deactivation and to develop some effective regeneration procedure in order to solve this issue.

4. Conclusions

Fe_3O_4 MNPs were successfully synthesized, and used as heterogeneous Fenton-like catalysts that can remove 2,4-DCP from aqueous solution efficiently. Two-stage first-order kinetics of 2,4-DCP degradation was observed in acidic condition, consisting of an induction period (first-stage) and a followed rapid degradation stage (second-stage). The induction time and the kinetic rate (k) of second-stage depended on pH, Fe_3O_4 MNPs dosage and temperature condition but less irrelevant to the concentrations of H_2O_2 and 2,4-DCP. Apparent activation energies of two stages were calculated as 66.0 kJ/mol (first-stage) and 28.8 kJ/mol (second-stage). The induction period was postulated as an activation process that involves dissolution of iron and activation of H_2O_2, while the

second-stage could mainly attributed to the bulk homogeneous Fenton reaction, which was further supported by the concentration of dissolved iron and ferrous ion in solution and the effect of radical scavengers. According to the aromatic intermediates, carboxylic acids and chloride ion determined by HPLC and IC, a possible degradation pathway based on •OH mechanism (especially free •OH in the bulk solution) was proposed. Although Fe_3O_4 MNPs would be of potential alternative for treatment of water contaminated with toxic organic compounds, the issue associated with the eventual loss of catalytic activity need to be further studied for its effective application.

Acknowledgements

The authors are grateful for the financial support provided by the National Natural Science Foundation of China (Grant Nos. 50978145; 51078210).

References

[1] M. Stieber, A. Putschew, M. Jekel, Environmental Science and Technology 45 (2011) 4944–4950.
[2] L.J. Xu, J.L. Wang, Journal of Hazardous Materials 186 (2011) 256–264.
[3] S. Navalon, M. Alvaro, H. Garcia, Applied Catalysis B: Environmental 99 (2010) 1–26.
[4] R. Gonzalez-Olmos, F. Holzer, F.D. Kopinke, A. Georgi, Applied Catalysis A 398 (2011) 44–53.
[5] J.H. Deng, J.Y. Jiang, Y.Y. Zhang, X.P. Lin, C.M. Du, Y. Xiong, Applied Catalysis B: Environmental 84 (2008) 468–473.
[6] W. Luo, L.H. Zhu, N. Wang, H.Q. Tang, M.J. Cao, Y.B. She, Environmental Science and Technology 44 (2010) 1786–1791.
[7] J.B. Zhang, J. Zhuang, L.Z. Gao, Y. Zhang, N. Gu, J. Feng, D.L. Yang, J.D. Zhu, X.Y. Yan, Chemosphere 73 (2008) 1524–1528.
[8] L.Q. Guo, F. Chen, X.Q. Fan, W.D. Cai, J.L. Zhang, Applied Catalysis B: Environmental 96 (2010) 162–168.
[9] G.B. Ortiz de la Plata, O.M. Alfano, A.E. Cassano, Applied Catalysis B: Environmental 95 (2010) 1–13.
[10] G.B. Ortiz de la Plata, O.M. Alfano, A.E. Cassano, Applied Catalysis B: Environmental 95 (2010) 14–25.
[11] S.P. Sun, A.T. Lemley, Journal of Molecular Catalysis A: Chemical 349 (2011) 71–79.
[12] S.S. Lin, M.D. Gurol, Environmental Science and Technology 32 (1998) 1417–1423.
[13] X.B. Hu, B.Z. Liu, Y.H. Deng, H.Z. Chen, S. Luo, C. Sun, P. Yang, S.G. Yang, Applied Catalysis B: Environmental 107 (2011) 274–283.
[14] A.L.T. Pham, C. Lee, F.M. Doyle, D.L. Sedlak, Environmental Science and Technology 43 (2009) 8930–8935.
[15] F. Haber, J. Weiss, Proceedings of the Royal Society A 134 (1934) 332–351.
[16] H. Yan, J.C. Zhang, C.X. You, Z.W. Song, B.W. Yu, Y. Shen, Materials Chemistry and Physics 113 (2009) 46–52.
[17] S.X. Zhang, X.L. Zhao, H.Y. Niu, Y.L. Shi, Y.Q. Cai, G.B. Jiang, Journal of Hazardous Materials 167 (2009) 560–566.
[18] X.F. Xue, K. Hanna, M. Abdelmoula, N.S. Deng, Applied Catalysis B: Environmental 89 (2009) 432–440.
[19] R. Massart, IEEE Transactions on Magnetics 17 (1981) 1247–1248.
[20] J.P. Jolivet, R. Massart, J.M. Fruchart, Nouveau Journal de Chimie (New Journal of Chemistry) 7 (1983) 325–331.
[21] S. Recillas, A. García, E. González, E. Casals, V. Puntes, A. Sánchez, X. Font, Desalination 277 (2011) 213–220.
[22] H. Tamura, K. Goto, T. Yotsuyan, M. Nagayama, Talanta 21 (1974) 314–318.
[23] C. Lee, C.R. Keenan, D.L. Sedlak, Environmental Science and Technology 42 (2008) 4921–4926.
[24] V. Kavitha, K. Palanivelu, Chemosphere 55 (2004) 1235–1243.
[25] J. Yan, S.B. Mo, J.R. Nie, W.X. Chen, X.Y. Shen, J.M. Hu, G.M. Hao, H. Tong, Colloids and Surfaces A: Physicochemical and Engineering Aspects 340 (2009) 109–114.
[26] Y.F. Zhu, W.R. Zhao, H.R. Chen, J.L. Shi, Journal of Physical Chemistry C 111 (2007) 5281–5285.
[27] J. Salado, M. Insausti, I. Gil de Muro, L. Lezama, T. Rojo, Journal of Non-Crystalline Solids 354 (2008) 5207–5209.
[28] J.P. Ge, Y.X. Hu, M. Biasini, W.P. Beyermann, Y.D. Yin, Angewandte Chemie International Edition 46 (2007) 4342–4345.
[29] M.L. Luo, D. Bowden, P. Brimblecombe, Applied Catalysis B: Environmental 85 (2009) 201–206.
[30] T.R. Gordon, A.L. Marsh, Catalysis Letters 132 (2009) 349–354.
[31] T. Zhou, Y.Z. Li, J. Ji, F.S. Wong, X.H. Lu, Separation and Purification Technology 62 (2008) 551–558.
[32] R. Oliveira, M.F. Almeida, L. Santos, L.M. Madeira, Industrial and Engineering Chemistry Research 45 (2006) 1266–1276.
[33] N.K. Daud, B.H. Hameed, Journal of Hazardous Materials 176 (2010) 938–944.
[34] N. Masomboon, C. Ratanatamskul, M.C. Lu, Environmental Science and Technology 43 (2009) 8629–8634.
[35] J.H. Ramirez, F.J. Maldonado-Hódar, A.F. Pérez-Cadenas, C. Moreno-Castilla, C.A. Costa, L.M. Madeira, Applied Catalysis B: Environmental 75 (2007) 312–323.
[36] H. Hassan, B.H. Hameed, Chemical Engineering Journal 171 (2011) 912–918.
[37] D.N. Thi, H.P. Ngoc, H.D. Manh, T.N. Kim, Journal of Hazardous Materials 185 (2011) 653–661.
[38] J. Herney-Ramirez, M. Lampinen, M.A. Vicente, C.A. Costa, L.M. Madeira, Industrial and Engineering Chemistry Research 47 (2007) 284–294.
[39] Q. Liao, J. Sun, L. Gao, Colloids and Surfaces A: Physicochemical and Engineering Aspects 345 (2009) 95–100.
[40] S.P. Sun, C.J. Li, J.H. Sun, S.H. Shi, M.H. Fan, Q. Zhou, Journal of Hazardous Materials 161 (2009) 1052–1057.
[41] C.P. Huang, Y.H. Huang, Applied Catalysis A 346 (2008) 140–148.
[42] J.Y. Feng, X.J. Hu, P.L. Yue, Environmental Science and Technology 38 (2004) 5773–5778.
[43] Z.Q. He, S. Song, H.P. Ying, L.J. Xu, J.M. Chen, Ultrasonics Sonochemistry 14 (2007) 568–574.
[44] S.T. Martin, A.T. Lee, M.R. Hoffmann, Environmental Science and Technology 29 (1995) 2567–2573.
[45] H. Wang, J.L. Wang, Applied Catalysis B: Environmental 89 (2009) 111–117.
[46] H. Wang, J.L. Wang, Electrochimica Acta 53 (2008) 6402–6409.
[47] W. Chu, C.Y. Kwan, K.H. Chan, S.K. Kam, Journal of Hazardous Materials 121 (2005) 119–126.
[48] E. Brillas, J.C. Calpe, J. Casado, Water Research 34 (2000) 2253–2262.
[49] C. Badellino, C.A. Rodrigues, R. Bertazzoli, Journal of Hazardous Materials 137 (2006) 856–864.
[50] C.C. Chen, P.X. Lei, H.W. Ji, W.H. Ma, J.C. Zhao, H. Hidaka, N. Serpone, Environmental Science and Technology 38 (2004) 329–337.
[51] J. Guo, M. Al-Dahhan, Applied Catalysis A 299 (2006) 175–184.